Shear Degradation Resistance of Star Polymers during Elongational Flow

L. Xue, U. S. Agarwal,* and P. J. Lemstra

Faculty of Chemical Engineering, Eindhoven University of Technology, 5600 MB, Eindhoven, The Netherlands

Received February 8, 2005; Revised Manuscript Received June 23, 2005

ABSTRACT: Linear high molecular weight polymers undergo central scission in strong flows due to buildup of stress from fluid drag. An alternative to linear architecture is the star branched polymer that shows higher shear stability against such scission. We consider two six-arm star polymers differing in the connectivity of the arms at the core. The first is a fused-core star PMMA, where the arms are interconnected at a triphenylene core, with the multiple bonds therein supporting one another against possible tensile fracture. The second is a linear-core star PMMA, containing linearly linked single bonds within the core as potential fracture sites under tensile stress. Their stress-induced scission tendency is analyzed during planar elongational flow of their dilute solutions in dibutyl phthalate in a cross-slot flow cell. We find that scission of the star PMMA at the arms dominates their degradation behavior, and both the linear-core and fused-core star PMMAs show similar flow-induced scission. These results are analyzed first in terms of the critical-stress-to-fracture (CSF) and then in terms of scission kinetics as described by the thermally activated barrier to scission (TABS). The experimentally observed scission kinetics of the arms can be represented by the TABS model, but a description of the core scission appears to demand consideration of several possible conformations of the branched polymers.

Introduction

Long chain flexible polymers in quiescent solutions exist as random coils that behave as rigid spheres of dimensions much larger than those predicted by their bulk density.[1] Therefore, even small concentration (c) of high molecular weight polymers can significantly enhance the viscosity of a solution (η) as compared to the viscosity of the solvent (η_s). Externally imposed strong flows result in changes in chain conformations, such as the coil−stretch transition from a randomly coiled state to stretched state at a critical strain rate $\dot{\epsilon}_{cs} \propto 0.5\tau^{-1}$, where τ is the longest relaxation time of the polymer.[1,2] Such conformational changes further introduce interesting behavior such as flow rate dependent viscosity (shear thinning and extensional thickening), elasticity, and normal stresses. Therefore, high molecular weight polymers are used for rheology modification applications, for example as lubricant additives[3] in automobiles, and for turbulent drag reduction[4] during oil transport. As these polymeric additives undergo stretching under the strong elongational flows encountered,[5−8] tensile stresses build up from chain ends toward chain center to an extent that the chains can undergo breakage at the center[9−15] and lose their rheology modification efficiency.

In a steady strong elongational flow (strain rate $\dot{\epsilon} > \dot{\epsilon}_{cs}$) of a dilute solution, a linear chain of $2N$ beads can be considered to be completely extended (Figure 1). The drag forces ($F_i = \xi V_i$, $V_i = \dot{\epsilon} x_i$) on the individual beads ($i = 1$, ..., N, at positions $x_i = ib$) add up, from the chain ends (bead number $i = N$) toward the chain center (bead number $i = 0$), to the tensile stresses in the ith segments as

$$\sigma_i = \sum_{N}^{i} F_i = \xi b \dot{\epsilon} (N^2 - i^2)/2 \qquad (1)$$

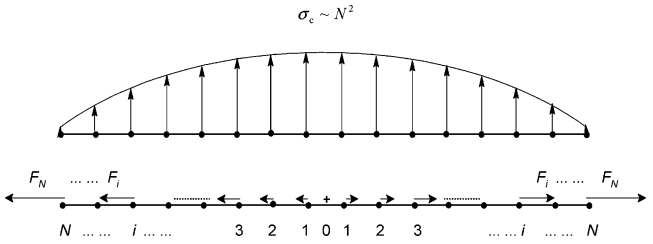

Figure 1. Parabolic distribution of tensile stresses (horizontal, but indicated in magnitude by the vertical arrows in the upper figure) in segments of a dissolved linear polymer chain fully extended due to fluid flow drag (shown as horizontal arrows in the lower figure) on the beads.

Here, b is the stretched segment length and ξ is the hydrodynamic drag coefficient of the beads. This cumulative stress has a maximum at the chain center:[9]

$$\sigma_c = \sigma_{i=0} = \xi b \dot{\epsilon} N^2/2 \qquad (2)$$

which scales with the square of the chain length. In an approach called critical stress to fracture (CSF), chain scission is considered to take place if the tensile stress (σ) in a segment exceeds the C−C single bond strength ($\sigma_f \sim 2.5-13.4$ nN),[9] i.e., if $\dot{\epsilon}$ is greater than a critical value which decreases with increasing chain molecular weight:

$$\dot{\epsilon}_f \sim N^{-2} \qquad (3)$$

High molecular weight, however, is often desired for high efficiency of rheology modification. Therefore, alternative macromolecular architectures are desired for reducing chain scission while retaining their high efficiency as rheology modifiers. Though several different polymeric topologies have been explored for their chain scission resistance characteristics, such effort largely appears to have been directed by availability of the architectures.[16−23] For example, branching or graft-

* To whom correspondence should be addressed. E-mail: u.s.agarwal@tue.nl.

10.1021/ma0502811 CCC: $30.25 © 2005 American Chemical Society
Published on Web 09/21/2005

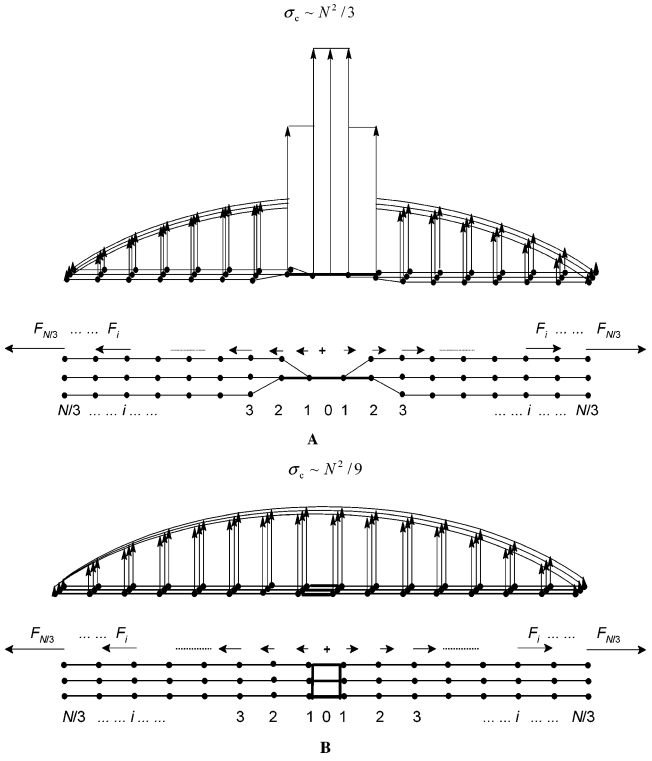

Figure 2. Elongational flow drag on the beads (shown as horizontal arrows) resulting in tensile stresses (magnitude indicated by the vertical arrows) in the segments of fully stretched six-arm star polymers with a linear core (**A**) and a fused core (**B**).

ing side chains to polymeric backbones is considered to enhance shear stability during turbulent flows and is attributed to sacrificial scission of the branches leading to only a small decrease in molecular weight.[17−19,22] However, our reanalysis shows that grafting on polymeric backbones may enhance the tensile stresses due to the additional drag on the grafts and thus reduce shear stability.[24]

An interesting class of branched polymers is star polymers because these have an elementary branching topology, with multiple linear chains linked to a single core. Kim et al.[17] found that a star polymer of structure **A** (Figure 2) was equally effective but more shear stable than a linear polymer (Figure 1) of the same molecular weight. Extending the CSF arguments of tensile stresses in fully stretched polymers (eq 2, $\sigma_c \sim N^2$, for linear polymers[9]), we attribute this to a smaller $\sigma_c \sim N^2/3$, in the star polymer **A** with a linear core (Figure 2) where the stresses ($\sim(N/3)^2$) in each of the three sets of arms add up to ($\sim N^2/3$) in the C−C single-bond linkages at the linear core. This has lead us to design a six-arm star polymer **B** (Figure 2) that is similar to structure **A**, but with the scission prone central single-bond linkages replaced by a fused core where the added up stress ($\sim N^2/3$) can be shared by several parallel linkages. In the event of an equivalent of three parallel linkages in the fused core (Figure 2, **B**), the tensile stress in each of the three parallel links would scale as ($\sigma_c \sim N^2/9$), making the structure **B** more stable than the structure **A**. Alternatively speaking, CSF thus predicts that for star polymers with structures **A** and **B** of identical molecular weight, with critical strain rates $\dot{\epsilon}_f^{(\mathbf{A})} \sim 3N^{-2}$ and $\dot{\epsilon}_f^{(\mathbf{B})} \sim 9N^{-2}$, respectively, there would exist strain rates $\dot{\epsilon}_f^{\mathbf{A-B}}$ intermediate between $\dot{\epsilon}_f^{(\mathbf{A})} \sim 3N^{-2}$ and $\dot{\epsilon}_f^{(\mathbf{B})} \sim 3\dot{\epsilon}_f^{(\mathbf{A})}$, where the star polymer **A** would undergo flow-induced scission at its linear core but the star polymer **B** with fused-core would be shear stable. The CSF further predicts scission at the arms for both the star polymers **A** and **B** at strain rates higher than $\dot{\epsilon}_f^{(\mathbf{B})}$ and no scission in either of the star polymers at strain rates lower than $\dot{\epsilon}_f^{(\mathbf{A})}$.

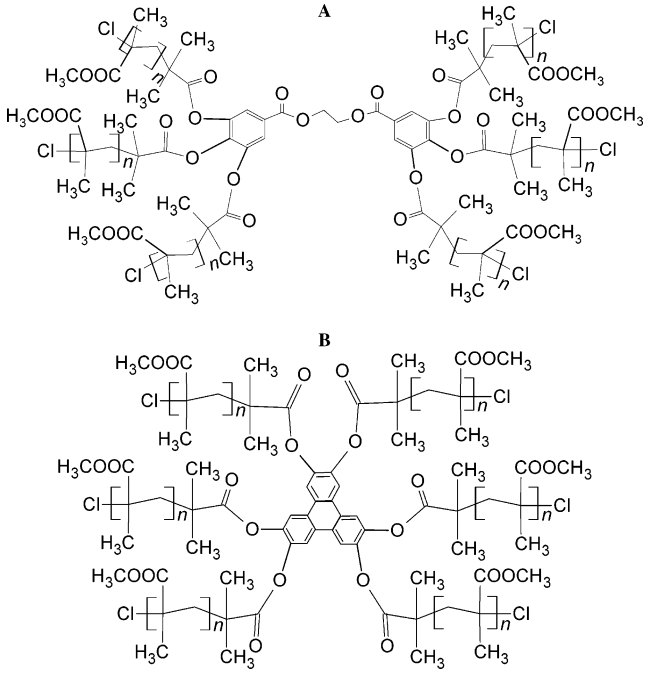

Figure 3. Chemical structures of the six-arm star PMMAs with a linear core (**A**) and a fused core (**B**), synthesized as described in ref 25.

Table 1. Weight-Average Molecular Weight ($\bar{M}_w$) and Polydispersity Index (PDI) of Star PMMAs and Their Cleaved Arms

	$\bar{M}_w/10^6$ (SEC-LS)		$\bar{M}_w/10^6$ (SEC)		PDI (SEC)	
sample	star	arm	star	arm	star	arm
linear-core star PMMA	2.10	0.37	1.19	0.34	1.26	1.18
fused-core star PMMA	2.35	0.36	1.32	0.34	1.30	1.16

We recently reported the design and synthesis of two six-arm star PMMAs with their core structures differing in the linking arrangement of the arms (Figure 3).[25] Here we examine if the consideration based on steady-state complete extension and CSF criteria indeed rule the flow-induced scission behavior of the star branched polymers. Chain scission behavior of these star polymers in dilute solution is studied experimentally during planar elongational flow in a cross-slot flow cell. The experimental results are compared with the theoretical predictions based not only on the CSF but also with the chain scission kinetics described by the thermally activated barrier to scission (TABS).

Experimental Section

Materials. Dibutyl phthalate (DBP, Aldrich, 99%) and acetone (Merck, AR) were used as received. Very high molecular weight linear-core star PMMA and fused-core star PMMA, with chemical structure **A** and **B**, respectively, as shown in Figure 3, were synthesized by core-first atom transfer radical polymerization as described in our previous report.[25] The molecular characteristics of the two star PMMAs, as determined by size exclusion chromatography (SEC) and by SEC coupled with light-scattering (SEC-LS), are reported in Table 1.

Preparation of Star PMMA Solution. Star PMMA (20 mg) was dissolved in acetone (4 mL). DBP (200 mL) was added

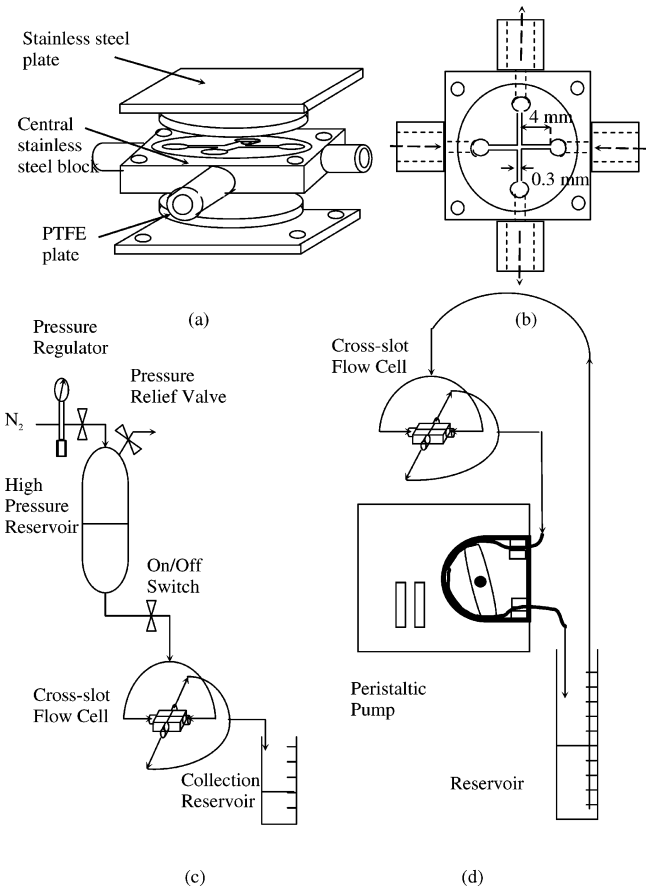

Figure 4. Schematic of (a) the construction of the cross-slot flow cell, and (b) the top view of the central block, and the flow arrangements for (c) high strain rate and (d) low strain rate experiments.

via a dropping funnel while stirring. Argon was bubbled through the solution for 1 h to remove acetone and yield a 100 ppm (w/v) solution of the star PMMA.

Cross-Slot Flow Cell. As shown in Figure 4a, the cross-slot flow cell was constructed from a central stainless steel block, with two round PTFE plates (2 mm thick) held in place with two rigid stainless steel plates (2.5 mm thick) clamped with four screws at the corners. Figure 4b shows the top view of the central block with a cross-slot of width $d = 0.3$ mm and depth $l = 2.5$ mm. The approach length to the slot was 4 mm. Each of the slots was connected to the external tubing (i.d. 4 mm) through a vertical cylindrical section (i.d. 3 mm) and a horizontal cylindrical section (i.d. 2 mm) as shown in Figure 4b.

Flow-Induced Scission Experiments. The high-pressure flow arrangement used for high strain rate ($\dot{\epsilon} > 25\,000$ s^{-1}) experiments is shown in Figure 4c. The star PMMA solution (200 mL) was filled into the high-pressure reservoir. For a desired volumetric flow rate (Q), a regulated nitrogen gas pressure (1−5 bar) was applied to the reservoir. The solution was lead through two opposing slots into the cross-slot flow cell, and then out through the other two opposing slots, to the collection reservoir. Q was determined from the measured flow time. The solution was returned to the upstream reservoir. The entire process was repeated for the desired number of passes.

The flow loop used for the low strain rate ($\dot{\epsilon} < 25\,000$ s^{-1}) experiments is shown in Figure 4d. A peristaltic pump downstream the cross-slot flow cell was used to continuously suck the solution from the reservoir, through the cross-slot flow cell, and returned to the reservoir. Q was determined by leading the solution flowing out of the peristaltic pump to an empty vessel and measuring the time required for flow of 50 mL solution.

Samples (20 mL each) were withdrawn from the reservoir after desired number of passes. To these samples, deionized water (0.1 mL) and n-heptane (30 mL) were added to precipitate the polymer which was recovered by centrifuging at 2500 rpm for 10 min. The polymer samples were then dissolved in tetrahydrofuran at a concentration of 0.5 mg mL^{-1} for SEC analysis.

Size Exclusion Chromatography (SEC). Polymer molecular weight and polydispersity were measured by SEC using a Waters GPC equipped with a Waters 510 pump, a Waters 410 differential refractometer (40 °C), a Waters WISP 712 autoinjector (50 μL injection volume), a PLgel (5 μm particle size) 50 mm × 7.5 mm guard column, and two PLgel mixed-C (5 μm particle size, for 200−2 × 10^6 g/mol) 300 mm × 7.5 mm columns (40 °C). Data acquisition and processing were performed using Waters Millennium 32 (v3.2) software. Tetrahydrofuran (THF, Biosolve, stabilized with BHT) was used as eluent at a flow rate of 1.0 mL/min. Calibration was done using polystyrene (PS) standards (Polymer Laboratories, 580 to 7.1 × 10^6 g mol^{-1}), and molecular weights were recalculated using the universal calibration principle and the Mark−Houwink parameters (PS: $K = 1.14 \times 10^{-4}$ dL g^{-1}, $\alpha = 0.716$; PMMA: $K = 0.944 \times 10^{-4}$ dL g^{-1}, $\alpha = 0.719$).[26]

Results and Discussion

Experimental Evaluation of the Scission Behavior. We are interested in evaluating the flow-induced scission tendency of the two six-arm star PMMAs: with a linear-core structure **A** containing linearly linked single bonds as the core and a fused-core structure **B** where the arms are connected to a triphenylene core (Figure 3). As seen from the $\bar{M}_w$ and PDI values of star PMMAs and their arms (Table 1), the two star PMMA samples have comparable average arm lengths and narrow molecular weight distributions. Solutions of each of the two polymers in DBP are prepared at a concentration of 100 ppm, about 2 orders of magnitude below the overlap concentration.[27] At the desired flow rate Q, a fresh solution is repeatedly flown through a cross-slot flow cell (Figure 4a). The solution undergoes first compression and then extension along perpendicular directions in the cross-slots (Figure 4b). The so-produced planar elongation flow has a stagnation region at the center of the cross-slots due to the symmetric geometry of the flow cell, and the nominal extensional strain rate is estimated as[9]

$$\dot{\epsilon} = \frac{Q}{d^2 l} \tag{4}$$

Parts a and b of Figure 5 show the SEC traces of the samples withdrawn during scission experiments at $\dot{\epsilon} =$ 46 800 s^{-1} for the star PMMAs with structures **A** and **B**, respectively. Curve a represents the zero sample taken before the scission experiments, and curves b−f represent samples withdrawn after 10, 20, 40, 80, and 120 passes. Arrow g represents the peak positions of the original star PMMA (curve a). Arrow h represents the peak position of the complete arms obtained by chemical cleavage (transesterification of the ester linkages connecting the arms to the core) of the arms.[25] We notice from Figure 5a,b that with increasing number of passes the molecular weight distribution of the scission product become bimodal. The area under the high molecular weight peak at arrow g corresponding to the original star PMMA decreases, with the appearance of a lower molecular weight peak. The emerging low molecular weight peaks in SEC curves b and c for 10 and 20 passes are located at arrow h, which represents

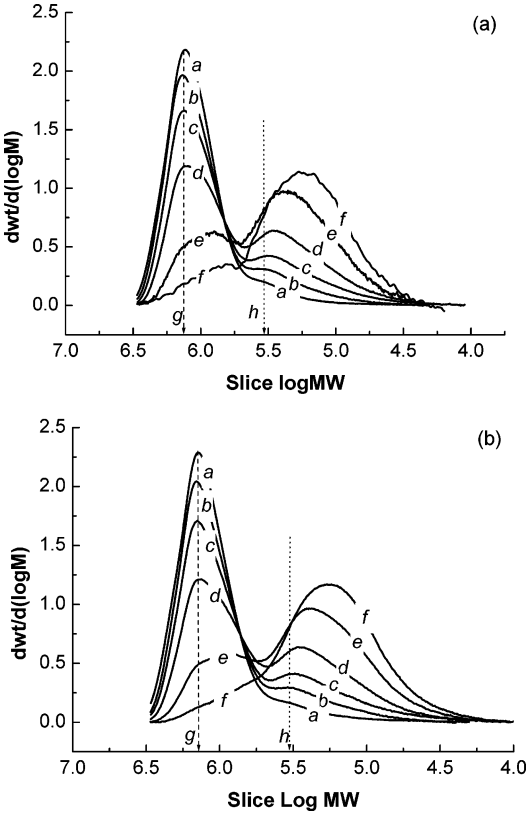

Figure 5. SEC traces of samples withdrawn during the scission analysis at $\dot{\epsilon} = 46\,800\ s^{-1}$ for star PMMA with (a) linear core and (b) fused core, through a cross-slot flow cell after different number of passes: *a*, 0; *b*, 10; *c*, 20; *d*, 40; *e*, 80; *f*, 120. Arrows *g* and *h* represent the peak positions of the original star molecules and the complete arms, respectively.

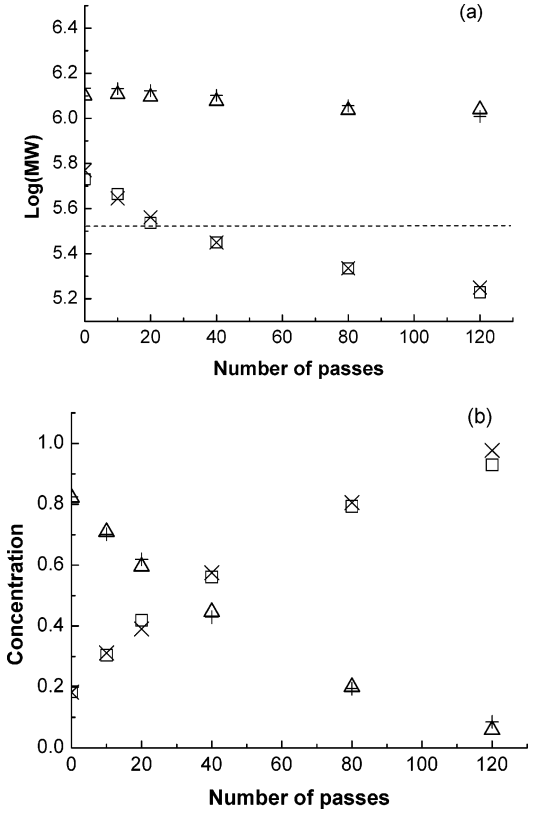

Figure 6. (a) Peak molecular weight and (b) the concentration of the partly degraded star molecules (△ and +) and arms (□ and ×) of linear-core star PMMA (△ and □) and fused-core star PMMA (+ and ×) samples during scission analysis at $\dot{\epsilon} = 46\,800\ s^{-1}$. The dashed line in (a) represents the peak position of the complete arms.

the SEC peak position of the complete arms. This suggests that detectable flow-induced scission of both the fused-core and the linear-core star PMMAs into arms takes place within first 10 passes at this strain rate. Even though the position of the high molecular weight peak remains unchanged near arrow *g* for the samples after 10 and 20 passes, increasing width of this peak with number of passes is clearly seen. This is because of the scission of a fraction of the original star PMMAs resulting in lower molecular weight star PMMAs, with fewer or shorter arms. Since the SEC measurements are based on universal calibration for linear polymers, these do not represent the true molecular weight of the star polymers. However, theoretical predictions of macromolecular volumes based on their conformations allow us to estimate the molecular weight of a star polymer (M_s) of known architecture (*f* arms) from the apparent molecular weight (M_l) in SEC calibrated with linear polymer:[28,29]

$$\frac{M_l}{M_s} = \left(\frac{f^{1/2}}{\sqrt{2}(f-1) - f + 2}\right)^{3/(1+\alpha)} \tag{5}$$

where α (=0.719 for PMMA in THF[26]) is the Mark–Houwink constant. This suggests that if the star polymer **A** of six arms were to break at its linear core into two star polymers of three arms each, the corresponding shift in the SEC peak would be $\Delta \log M = 0.17$. We see absence of such a shift in the position of the high molecular weight peak even in the curves *d* at 40 passes where a large fraction (~40 wt %) of the original polymer has been converted into arms, suggesting that scission at the linear core, if at all present, is not the prominent mode of flow-induced scission during the applied flow of $\dot{\epsilon} = 46\,800\ s^{-1}$. Further, the SEC curves of the scission products of linear-core and fused-core star PMMAs in Figure 5a,b are very similar, implying their similar flow-induced scission characteristics. The apparent lack of influence of the core structure favors the conclusion that chain scission is primarily located at the arms for both the star PMMAs.

With increasing number of passes beyond 40 passes, we find that the low molecular weight peak shifts to molecular weights lower than that corresponding to complete arms (shown by arrow *h*). This indicates the possible secondary scission of the once broken arms or scission of the arms at locations away from their linkages to the cores.

The SEC traces in Figure 5a,b were then resolved into two Gaussian peaks (by fitting with the multipeaks feature in the graphics software Origin 6.0): a high molecular weight peak near arrow *g* corresponding to the original star polymer peak and a low molecular weight peak near arrow *h* corresponding to the scission product peak. The area under each of the two resolved peaks represents the concentration of the corresponding polymer species, allowing us to calculate the extent of conversion (weight fraction) of the star PMMA into arms. The SEC molecular weight of the peak corresponding to the original six-arm star polymers decreases only marginally with number of passes (Figure 6a) due to the relatively small dependence of the star molecular size on the number of arms.[30] However, the increasing conversion of the original star molecules into linear

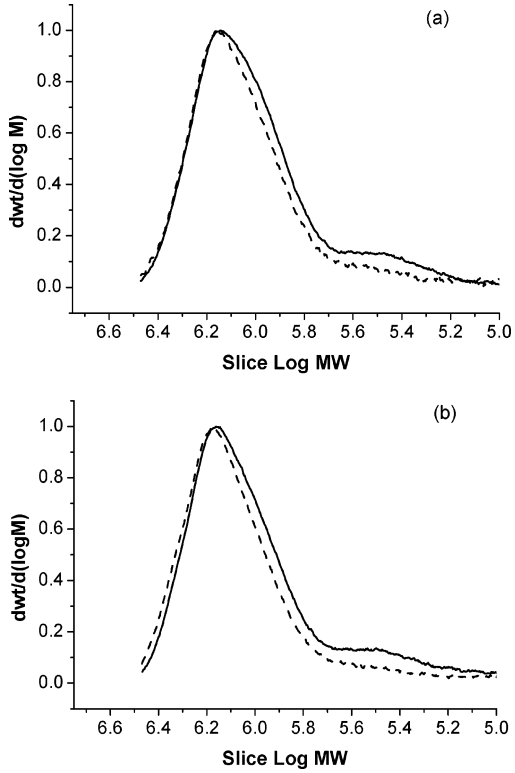

Figure 7. SEC traces of starting star samples (dashed lines) and samples withdrawn after 60 passes (solid lines) during the scission analysis at $\dot{\epsilon} = 27\,800\ s^{-1}$ for star PMMA with (a) linear core and (b) fused core.

arms with increasing number of passes is clearly seen from the trends of the corresponding weight fractions in Figure 6b. For the low molecular weight peak corresponding to cleaved arms, the peak molecular weight decreases with increasing number of passes (Figure 6a). This is related either to the aforementioned secondary scission of the once cleaved long arms or to the slower scission of the shorter arms among the distribution of the arm lengths present in the original sample.

If the linear-core star PMMA were to undergo scission at the single-bond linkages in its core so as to generate three-arm star molecules, a higher rate of overall flow-induced scission will be expected for the linear-core star PMMA as compared to the fused-core star PMMA. But Figure 6 suggests that the overall rates of conversion of the two original star PMMAs into scission products are very similar.

As discussed in the Introduction, it is possible that the applied strain rate $\dot{\epsilon} = 46\,800\ s^{-1}$ is so high ($> \dot{\epsilon}_f^{(\mathbf{B})}$) that arm scission dominates the flow-induced degradation of both the linear-core and the fused-core star molecules. Since CSF predicts only core scission, and that only in linear-core star polymer **A**, at strain rates $\dot{\epsilon}_f^{\mathbf{A-B}}$ intermediate between $\dot{\epsilon}_f^{(\mathbf{A})} \sim 3N^{-2}$ and $\dot{\epsilon}_f^{(\mathbf{B})} \sim 3\dot{\epsilon}_f^{(\mathbf{A})}$, we carried out flow-induced scission experiments at a lower strain rate: $\dot{\epsilon} = 27\,800\ s^{-1}$. Figure 7a,b shows that even after 60 passes there is again no discernible difference in the scission tendency between these two core structures. The shifts in the high molecular weight peak, as well as the fraction of the emerging low molecular weight peak, are both similar for the two star PMMAs. To further examine the possibility of only the core scission in the linear-core star PMMA, its flow-induced scission experiments were carried out at even

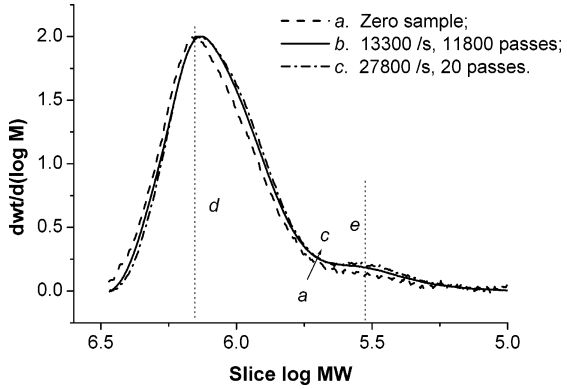

Figure 8. SEC traces of linear-core star PMMA during chain scission analysis at different strain rates and number of passes. Zero sample (dashed line *a*); at $\dot{\epsilon} = 13\,300\ s^{-1}$ after 11 800 passes (solid line *b*); at $\dot{\epsilon} = 27\,800\ s^{-1}$ after 20 passes (dash−dotted line *c*). Arrows *d* and *e* represent the peak positions of the original star polymer and the complete arms, respectively.

lower strain rate: $\dot{\epsilon} = 13\,300\ s^{-1}$. Figure 8 shows that the SEC curve of the sample after 11 800 passes at $\dot{\epsilon} = 13\,300\ s^{-1}$ overlaps closely with the SEC curve of the sample after 20 passes at $\dot{\epsilon} = 27\,800\ s^{-1}$. Thus, the apparent nature of scission (arm scission vs core scission) remains the same even at $\dot{\epsilon} = 13\,300\ s^{-1}$, where the scission rate is very low, requiring 11 800 passes for only ~4 wt % scission into arms. Considering that this experiment required over 7 days of continuous pumping of the polymer solution with the peristaltic pump, and an experiment for similar time at $\dot{\epsilon} = 9800\ s^{-1}$ failed to show any detectable scission, we concluded inability to carry out meaningful scission experiments at this and lower strain rates with our cross-slot flow cell. Clearly, arm scission seems to dominate the flow-induced scission behavior of both the linear-core and fused-core star PMMAs in the experimentally accessible range of strain rates.

It is important to ensure that we are examining the polymer scission behavior at center of the cross-slot, and not elsewhere in the flow/cell system, such as at the entry to the cross-slot. For this purpose, the PTFE plates (Figure 4a) were temporarily replaced with similar plates but with central holes of id 4 mm that allowed the flowing solution to bypass the stagnation zone of the cross-slot. Curve *b* in Figure 9 shows the SEC of the sample after 10 passes at ($\dot{\epsilon} = 46\,800\ s^{-1}$), and its close overlap with the SEC curve *a* of the original sample suggests negligible chain scission, in contrast to the obvious scission into arms seen in SEC curve *c* after similar flow through the stagnation zone region. Thus, the chain scission observed in our experiments can indeed be attributed to the planar elongation flow in the central region of the cross-slots.

The initial rate of scission into arms at different strain rates was estimated from the SEC determined weight fraction (w) of the arms in the withdrawn sample and the corresponding number of passes (n):

$$R_{\text{arm}} = \frac{wQ}{nd^2l} \tag{6}$$

Since only a small fraction of the molecules passing through the flow cell experience the elongational flow of sufficient strength at the stagnation point,[12] and there is even a concern about the location of the site of scission

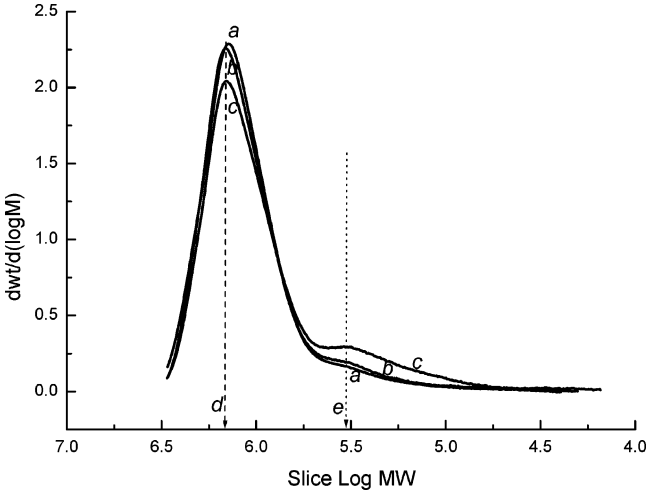

Figure 9. SEC traces of samples withdrawn during the scission analysis at $\dot{\epsilon} = 46\,800\ s^{-1}$ for fused-core star PMMA: *a*, zero sample; *b*, 10 passes through the flow system while bypassing the center of the cross-slot; *c*, 10 passes through cross-slot flow cell. Arrows *d* and *e* represent the peak positions of the original star molecules and the arms, respectively.

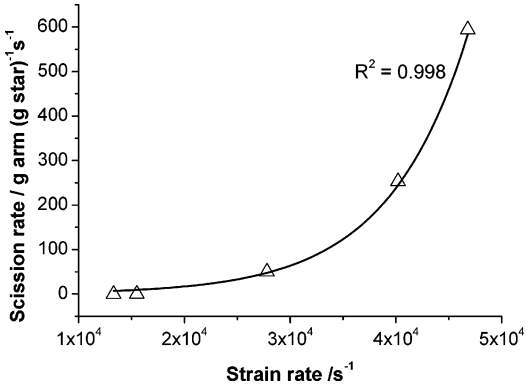

Figure 10. Initial scission rate vs nominal strain rate (eq 4) for the linear-core star PMMA. Symbols represent the experimental data (eq 6). Solid line represents the fit to exponential dependence (eq 7).

Table 2. Rates of Arm and Core Scission of the Linear-Core Star PMMA at Different Strain Rates

strain rate/s^{-1}	*n*/passes	*w*	R_{arm}/g arms (g star)$^{-1}$ s^{-1}	$R_{linear-core}/R_{arm}$[a]
13 300	11808	0.034	3.86×10^{-2}	0.057
15 500	11340	0.056	7.6×10^{-2}	0.110
27 800	20	0.036	50	3.88
40 200	20	0.126	253.3	126
46 800	10	0.127	594.4	775

[a] Predicted from eq 11.

within the cross of the cross-slot,[14] the scission rate as calculated above is only representative. Several measured weight fractions of the scission product and the corresponding number of passes for the linear-core star PMMA are presented in Table 2. When the initial arm scission rate R_{arm} is plotted in Figure 10 as a function of the strain rate, we notice that it increases rapidly with strain rate, and we represent it by the following exponential function:

$$R_{arm} = C_1 \exp(C_2\dot{\epsilon}) \tag{7}$$

obtaining the fitted parameters (corresponding to the shown as solid line in Figure 10) as $C_1 = 1.22$ g arms (g star)$^{-1}$ s^{-1} and $C_2 = 1.33 \times 10^{-4}$ s.

Thermally Activated Barrier to Scission (TABS) Approach. This access to the flow-induced scission rate R_{arm} and the exponential dependence of R_{arm} on the strain rate prompted us to analyze our observations in terms of the TABS description of the kinetics of scission of polymer chains in steady elongational flows. In the original form of this description, the scission rate of the *i*th backbone bond (Figure 1) of a linear polymer was considered as an Arrhenius type thermally activated process,[31,32] with the flow-induced stress (σ_i, eq 1) reducing the thermal activation energy barrier from its equilibrium value (U_0):

$$k_i = \nu_0 \exp[-U_0/(k_BT) + a\sigma_i/(k_BT)] \sim \nu_0 \exp[-U_0/(k_BT) + (a/b)\beta(N^2 - i^2)/2] \tag{8}$$

where ν_0 is a characteristic vibrational frequency of a bond, k_B is the Boltzmann's constant, T is the temperature, a is the stretched bond length scale, the dimensionless strain rate is $\beta = C\eta_s b^3\dot{\epsilon}/k_BT$, and $C = 2\pi/\ln i$. It thus predicts that the chain scission is not precisely central, but the chain scission probability distribution is Gaussian with a maximum at the chain center. The total scission rate in the three pairs of the fully extended star polymer arms, each of N_{arm} monomers, can be obtained as

$$R_{arm} = 3\sum_{i=1}^{N_{arm}} k_i = \nu_0' 3(\pi b/2a\beta)^{0.5} \exp[-U_0/k_BT] \exp[(a/b)\beta {N_{arm}}^2/2] \tag{9}$$

where ν_0' is the effective bond frequency which is lower than the unperturbed value ν_0 and has a small dependence on the stress.[31] The experimental exponential factor $C_2 = 1.33 \times 10^{-4}$ s is in order of magnitude agreement with the calculated value ($\sim 3.6 \times 10^{-4}$ s) of $(a/b)\beta {N_{arm}}^2/2\dot{\epsilon}$. This indicates that the shear stability of the star architecture is arm length dependent.

When all arms are extended in linear-core star polymer, the scission rate of the $q = 7$ single-bond linkages under stress $\sigma = 3\sigma_{arm}$ can be obtained as

$$R_{linear-core} = q\nu_0' \exp[-U_0/k_BT] \exp[(a/b)3\beta {N_{arm}}^2/2] \tag{10}$$

Then the ratio of the total scission rates of the linear-core to arms is predicted as

$$R_{linear-core}/R_{arm} = (q/3)(2a\beta/\pi b)^{0.5} \exp[(a/b)\beta {N_{arm}}^2] \tag{11}$$

i.e., preference for the linear-core scission over the arm scission at the high strain rates and long arm lengths. Neglecting the small strain rate dependence of the preexponential factor of eq 7 and then comparing it with eq 9 results in

$$C_2 = (a/b)(\beta/\dot{\epsilon}){N_{arm}}^2/2 \tag{12}$$

and substitution into eq 11 yields

$$R_{linear-core}/R_{arm} = \psi(q/3)(2a\beta/\pi b)^{0.5} \exp(2C_2\dot{\epsilon}) \tag{13}$$

where we have introduced a factor ψ to account for the probability that when all six arms are stretched from

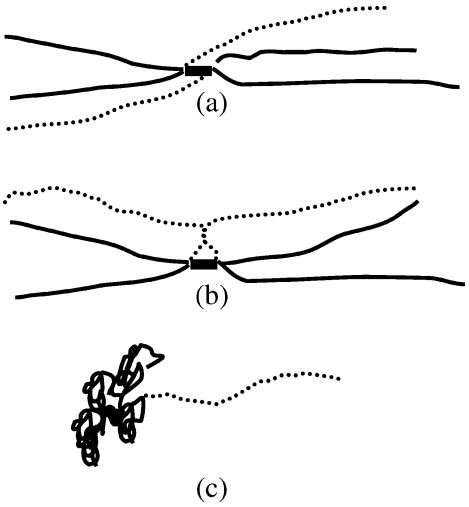

Figure 11. Schematic of some probable stretching conformations of the six-arm star polymers, with the two arms (dotted arms) (a) stretched so as not to favor core scission (as compared to Figure 2, **A**), (b) with interarm entanglements, and (c) with only one arm (dotted arm) stretched during the transient process.

the core, they may not be necessarily oriented so as to result in adding up of the stresses at the single-bond linkages in the linear core. For example, Figure 11a shows one such possible conformation. In fact, among fully stretched six-arm star conformations, the probability of the linear-core scission assisting conformation can be calculated as $\psi = 1/10$. The so computed value of $R_{\text{linear-core}}/R_{\text{arm}}$ for our experiments are shown in Table 2, and these suggest a preference for the linear-core scission over the arm scission at high strain rates. Thus, the TABS predictions are in line with the CSF predictions, but we did not observe this phenomenon in our experiments. Further, we observed similar scission tendency of the linear-core and fused-core star PMMAs. This may due to the oversimplified assumption that arm scission in a star molecule can occur only after complete extension of all its six arms. For example, interarm entanglements, such as the one shown in Figure 11b, would result in the stress in the linear-core bonds no higher than the stress in the arm bonds. If it were possible to account for the probability of the extended conformations free from such entanglements, we would have additional reduction in the predicted values of $R_{\text{linear-core}}/R_{\text{arm}}$, perhaps by orders of magnitude. Rabin,[33] and Nguyen and Kausch[34] argued that the chain extension may not be complete, and the critical strain rate to fracture in the polymer chains may not decrease as $\dot{\epsilon}_f \sim N^{-2}$ (eq 3) but only as $\dot{\epsilon}_f \sim N^{-1}$. Even in the case of cross-slot flows, Mohammad et al.[12] found a $\dot{\epsilon}_f \sim N^{-1}$ scaling at Reynold's number exceeding 1000. However, the corresponding theory is still in the stage of early development.[14,34] In addition, direct visualization of DNA molecules in flows having stagnation point have shown that formation of folds during strong extensional flows hinder the complete extension of the chain molecules.[35,36] Similar behavior has been detected during molecular simulations.[8,37−40] In their simulations of star polymers in elongational flows, Cifre et al. noticed that the arms undergo "coil−stretch" transition at different times.[30] Before the six-arm star polymer molecule experiences sufficient strain for stretching of all its arms, extension of fewer arms of the six-arm star polymer would result in a smaller stress at the core, a smaller value of $R_{\text{linear-core}}/R_{\text{arm}}$, and thus a reduced preference for the scission of linear core. For example, the stretching of a single arm before extension of the rest of the arms (Figure 11c) can make it vulnerable to flow-induced arm scission, without inducing similar scission of the linear core. Thus, there are several additional features that need to be accounted for before the TABS theory can possibly enable prediction of the flow-induced scission behavior of branched polymers.

Conclusions

We have evaluated the flow-induced scission behavior of six-arm star PMMAs during planar elongational flow of their dilute solutions in DBP in a cross-slot flow cell. We find that the bond scission is located primarily in the arms, even when the core of the star PMMA consists of single-bond linkages. This is in disagreement with the CSF prediction that the accumulation of stress from the three pairs of arms would make the core vulnerable. Qualitative arguments based on several possible highly extended conformations, as well as incomplete stretching of all arms, are presented to explain the experimental observations. From the kinetics point of view, the experimental scission behavior of arms can be represented by the TABS model, but similar prediction of the core scission seems to demand additional developments to account for the several possible topological conformations.

Acknowledgment. We thank Wieb Kingma for SEC measurements.

References and Notes

(1) de Gennes, P. G. *Scaling Concepts in Polymer Physics*; Cornell University Press: Ithaca, NY, 1979; pp 30, 181.
(2) Schroeder, C. M.; Babcock, H. P.; Shaqfeh, E. D. G.; Chu, S. *Science* **2003**, *301*, 1515.
(3) Ver Strate, G.; Struglinski, M. J. *Polymers as Rheology Modifiers*; Schultz, D. N., Glass, J. E., Eds.; ACS Symposium Series 462; American Chemical Society: Washington, DC, 1991; Chapter 15, p 256.
(4) Schulz, D. N.; Kitano, K.; Duvdevani, I.; Kowalik, R. M.; Eckert, J. A. In *Polymers as Rheology Modifiers*; Schultz, D. N., Glass, J. E., Eds.; ACS Symposium Series 462; American Chemical Society: Washington, DC, 1991; Chapter 10, p 176.
(5) de Gennes, P. G. *J. Chem. Phys.* **1974**, *60*, 5030.
(6) Hinch, E. J. *Phys. Fluids* **1977**, *20*, 522.
(7) Agarwal, U. S.; Bhargava, R.; Mashelkar, R. A. *J. Chem. Phys.* **1998**, *108*, 1610.
(8) Agarwal, U. S. *J. Chem. Phys.* **2000**, *113*, 3397.
(9) Odell, J. A.; Keller, A. *J. Polym. Sci., Polym. Phys.* **1986**, *24*, 1889.
(10) Nguyen, T. Q.; Kausch, H. H. *Adv. Polym. Sci.* **1992**, *100*, 73.
(11) Horn, A. F.; Merrill, E. W. *Nature (London)* **1984**, *312*, 140.
(12) Islam, M. T.; Vanapalli, S. A.; Solomon, M. J. *Macromolecules* **2004**, *37*, 1023.
(13) Buchholz, B. A.; Zahn, J. M.; Kenward, M.; Slater, G. W.; Barron, A. E. *Polymer* **2004**, *45*, 1223.
(14) Hsieh, C.-C.; Park, S. J.; Larson, R. G. *Macromolecules*, in press.
(15) Agarwal, U. S.; Mashelkar, R. A. *J. Chem. Phys.* **1994**, *100*, 6055.
(16) Ting, R. Y.; Little, R. C. *Nat. Phys. Sci.* **1973**, *241*, 42.
(17) Kim, O. K.; Little, R. C.; Patterson, R. L.; Ting, R. Y. *Nature (London)* **1974**, *250*, 408.
(18) Roovers, J. *Encyclopedia of Polymer Science and Engineering*; Wiley: New York, 1986; Vol. 2, p 478.
(19) Ungeheuer, S.; Bewersdorff, H. W.; Singh, R. P. *J. Appl. Polym. Sci.* **1989**, *37*, 2933.
(20) Ver Strate, G. W.; Kresege, E. N.; Graessley, W. W. Ger. Pat. 3,013,318, Oct 30, 1980.
(21) Choi, S. U. S.; Cho, Y. I.; Kasza, K. E. *J. Non-Newt. Fluid Mech.* **1992**, *41*, 289.
(22) Agarwal, S. H.; Jenkins, R. F.; Porter, R. S. *J. Appl. Polym. Sci.* **1982**, *27*, 113.
(23) Morgan, S. E.; McCormick, C. L. *Prog. Polym. Sci.* **1990**, *15*, 103.

(24) Agarwal, U. S.; Mashelkar, R. A. *J. Non-Newt. Fluid Mech.* **1994**, *54*, 1.
(25) Xue, L.; Agarwal, U. S.; Zhang, M.; Staal, B. B. P.; Müller, A. H. E.; Bailly, C. M. E.; Lemstra, P. J. *Macromolecules* **2005**, *38*, 2093.
(26) Beuermann, S.; Paquet, D. A., Jr.; McMinn, J. H.; Hutchinson, R. A. *Macromolecules* **1996**, *29*, 4206. Kirkland, J. J.; Rementer, S. W. *Anal. Chem.* **1992**, *64*, 904.
(27) $c^* \approx 3M/4\pi R_g^3 N_A \sim 8700$ ppm, where $M \sim 2.3 \times 10^6$, $R_g \sim 45$ nm (ref 24), and $N_A \sim 6 \times 10^{23}$.
(28) Rudin, A.; Grinshpun, V.; O'Driscoll, K. *J. Liq. Chromatogr.* **1984**, *7*, 1809.
(29) Radke, W. *Macromol. Theory Simul.* **2001**, *10*, 668.
(30) Hernández Cifre, J. G.; López Martínez, M. C.; García de la Torre, J. *J. Non-Cryst. Solids* **2002**, *307*−*310*, 818−823.
(31) Odell, J. A.; Keller, A.; Rabin, Y. *J. Chem. Phys.* **1988**, *88*, 4022.
(32) Odell, J. A.; Carrington, S. P. In *Flexible Polymer Chain Dynamics in Elongational Flow, Theory and Experiment;* Nguyen, T. Q., Kausch, H. H., Eds.; 1999; Chapter 7, p 177.
(33) Rabin, Y. *J. Chem. Phys.* **1987**, *86*, 5215.
(34) Nguyen, T. Q.; Kausch, H.-H. *Makromol. Chem.* **1989**, *190*, 1389.
(35) Perkins, T. T.; Smith, D. E.; Chu, S. *Science* **1997**, *276*, 2016.
(36) Smith, D. E.; Chu, S. *Science* **1998**, *281*, 1335.
(37) Larson, R. G.; Hu, H.; Smith, D. E.; Chu, S. *J. Rheol.* **1999**, *43*, 267.
(38) Rallison, J. M.; Hinch, E. J. *J. Non-Newtonian Fluid Mech.* **1988**, *29*, 37.
(39) Larson, R. G. *Rheol. Acta* **1990**, *29*, 371.
(40) Hinch, E. J. *J. Non-Newtonian Fluid Mech.* **1994**, *54*, 209.

MA0502811